JACC: CARDIOVASCULAR INTERVENTIONS
VOL. 8, NO. 15, 2015

ISSN 1936-8798/$36.00
PUBLISHED BY ELSEVIER INC.
http://dx.doi.org/10.1016/j.jcin.2015.09.015

PERIPHERAL

Pulmonary Artery Denervation Attenuates Pulmonary Arterial Remodeling in Dogs With Pulmonary Arterial Hypertension Induced by Dehydrogenized Monocrotaline

Ling Zhou, MD,* Juan Zhang, MD,* Xiao-Min Jiang, MD,† Du-Jiang Xie, MD,* Jin-Song Wang, MD,* Li Li, MD,* Bin Li, PHD,† Zhi-Mei Wang, MD,‡ Alexander M.K. Rothman, MD,§ Allan Lawrie, PHD,§ Shao-Liang Chen, MD*‡

ABSTRACT

OBJECTIVES This study aimed to investigate sympathetic nerve (SN) ultrastructural changes and hemodynamic and pulmonary artery (PA) pathological improvements by pulmonary arterial denervation (PADN) in animals with pulmonary arterial hypertension (PAH), as well as the underlying mechanisms.

BACKGROUND SN overactivity plays a role in PAH. Previous studies have reported short-term improvements in pulmonary arterial pressure (PAP) and cardiac function by PADN, but PA remodeling and the associated mechanisms remain unclear.

METHODS Forty dogs were randomly (ratio of 1:3) assigned to the control (intra-atrial injection of N-dimethylacetamide, 3 mg/kg) and test (intra-atrial injection of dehydrogenized-monocrotaline, 3 mg/kg) groups. After 8 weeks, the animals in the test group with a mean PAP >25 mm Hg ($n = 20$) were randomized (ratio of 1:1) into the sham and PADN groups. At 14 weeks, the hemodynamics, medial wall thickness and PA muscularization, and messenger ribonucleic acid expression of genes in lung tissues were measured. Another 35 PAH dogs were used to measure the SN conduction velocity, electron microscopic assessment, and nerve distribution.

RESULTS PADN induced significant SN demyelination and axon loss and slowed SN conduction velocity over time, with resulting profound reductions in the mean PAP (23.5 ± 2.3 mm Hg vs. 33.7 ± 5.8 mm Hg), pulmonary vessel resistance (3.5 ± 2.3 Wood units vs. 7.7 ± 1.7 Wood units), medial wall thickness (22.3 ± 3.3% vs. 30.4 ± 4.1%), and full muscularization (40.3 ± 9.3% vs. 57.1 ± 5.7%) and increased nonmuscularization (29.8 ± 6.1% vs. 12.9 ± 4.9%) compared with the Sham group (all $p < 0.001$). PADN inhibited the messenger ribonucleic acid expression of genes correlated with inflammation, proliferation, and vasoconstriction.

CONCLUSIONS PADN induces permanent SN injury and subsequent improvements in hemodynamics and PA remodeling in animals with PAH through mechanisms that may be experimentally and clinically beneficial.
(J Am Coll Cardiol Intv 2015;8:2013–23) © 2015 by the American College of Cardiology Foundation.

From the *Division of Cardiology, Nanjing First Hospital, Nanjing Medical University, Nanjing, China; †Department of Cardiovascular Research, Nanjing Medical University, Nanjing, China; ‡Division of Cardiology, Nanjing Heart Center, Nanjing, China; and the §Department of Cardiovascular Science, University of Sheffield, Sheffield, United Kingdom. This study was granted by National Natural Scientific Funding of China (NSF81270191) and Jiangsu Provincial Outstanding Medical Program (BL20142338). Dr. Rothman has received research funding from Medtronic; and has received consulting fees from SoniVie. Dr. Chen is the fellow of the Collaborative Innovation Center for Cardiovascular Disease Translational Medicine and Clinical Medical Research Center of Jiangsu Province, China. The first two authors contributed equally to this work. All other authors have reported that they have no relationships relevant to the contents of this paper to disclose.

Manuscript received July 14, 2015; revised manuscript received September 21, 2015, accepted September 21, 2015.

ABBREVIATIONS AND ACRONYMS

MWT = medial wall thickness

PA = pulmonary artery

PADN = pulmonary artery denervation

PAH = pulmonary arterial hypertension

PAP = pulmonary arterial pressure

RV = right ventricle/ventricular

SN = sympathetic nerve

Pulmonary arterial hypertension (PAH) is a diverse group of diseases characterized by progressive pulmonary vascular remodeling and right ventricular (RV) failure and defined by a resting mean pulmonary arterial pressure (mPAP) ≥25 mm Hg (1-3). Current treatments are limited to pharmacological vasodilation and antiproliferation (4-7); however, persistent pulmonary artery (PA) remodeling puts many patients at risk of death (5-7).

The innervation of the PA is predominantly sympathetic (8), and increased sympathetic nerve (SN) activity and circulating catecholamines (9-11) have been demonstrated in patients with PAH, suggesting that SN overactivation plays a critical role in PAH. Trials targeting sympathetic activation have been undertaken; however, in contrast to left heart failure, nonselective beta-blockers reduce exercise capacity and worsen hemodynamics in patients with PAH (1,12,13). This outcome may be explained by the complex innervation of the PA and the variety of neurotransmitters and cotransmitters delivered to the pulmonary vasculature (8,14,15). Surgical denervation of the pulmonary artery abolishes the increase in pulmonary arterial pressure (PAP) induced by PA extension in experimental models (16). This effect has also been demonstrated using percutaneous pulmonary artery denervation (PADN) to abolish balloon inflation-induced increases in PA pressure in a dog model (17) and in patients with PAH (18). However, little published data demonstrates the pathological improvements and the associated mechanisms of PADN (19). Accordingly, the current study aimed to investigate: 1) whether PADN induces persistent SN injury; 2) whether hemodynamics improvements by PADN are accompanied by a subsequent improvement of PA remodeling; and 3) whether PADN reduces inflammation, abnormal proliferation, and vasoconstriction, 3 major mechanisms that are correlated with the progression of PA remodeling in an experimental PAH model.

SEE PAGE 2024

METHODS

EXPERIMENTAL ANIMALS. The study protocol was approved by the Institutional Animal Care and Use Committee, in accordance with the Guide for the Care and Use of Laboratory Animals (National Research Council). The animals had free access to food and water and were housed in a room with a 12:12-h light-dark cycle at 20°C to 24°C.

Forty adult beagle dogs (≥3 months of age, body weight 8 to 10 kg, Nanjing Medical University Animal Laboratory) were randomly assigned to 2 groups after the first hemodynamic measurement: control (n = 10, intra-atrial injection of N-dimethylacetamide, 3 mg/kg) and test (n = 30, intra-atrial injection of dehydrogenized monocrotaline [DHMCT], 3 mg/kg). Eight weeks after the injection, repeat hemodynamic measurements were performed. Animals in the test group with an mPAP >25 mm Hg were randomly divided into sham (n = 10, PADN catheter was positioned in the PA and connected with a generator, but without ablation) and PADN (n = 10, PADN procedure was performed for all animals). After an additional 6 weeks, the final hemodynamic measurement was performed, all animals were sacrificed, and all lung tissues with PA vasculature were stored at −80°C for pathological and molecular studies. SN trunks of the PA from another 41 animals with or without injection of DHMCT were isolated for the measurement of sympathetic nerve conduction velocity (SNCV) and evaluation by electron microscopy (**Figure 1**).

HEMODYNAMIC MEASUREMENTS. The hemodynamic measurements have been described previously (17,18). Briefly, at 14 weeks, a 7-F sheath was inserted into the femoral vein, and a Swan-Ganz catheter (Edwards Lifesciences, Irvine, California) was positioned at the distal PA.

PADN PROCEDURE. Following randomization, the animals were treated with aspirin (900 mg/day) and clopidogrel (300 mg/day). PADN has been described previously (17) and modified in this study (**Figures 2A to 2C**). Briefly, a 7-F PADN catheter was positioned at the conjunctional area between the distal main PA and the ostial left PA. At each point, ablation was performed with the following parameters: a temperature of 45°C to 50°C, energy ≤10 W, and time of 120 s.

TYROSINE HYDROXYLASE IMMUNOSTAINING. The animals were killed with an intraperitoneal injection of sodium pentobarbital (50 mg/kg). The PA with its surrounding adipose and connective tissue was cleared of blood via an intravascular phosphate-buffered saline bolus and immediately fixed with 4% paraformaldehyde for 24 h.

PA tissues were divided into 3 segments (the main PA trunk, 5 mm in length, and the proximal right and left PA, each 1 cm in length) and were sliced at a thickness of 5 μm. PA slices were then counterstained

with hematoxylin. The tissues were examined using a Leica TSL laser confocal microscope (Leica Microsystems Inc., Bannockburn, Illinois), and the distance from the nerve endings to the PA vessel walls was measured.

3-DIMENSIONAL RECONSTRUCTION OF PA AND SYMPATHETIC NERVES. All of the images of SN staining with PA vessel walls were converted into grayscale from RGB, repeat coded with Grim software (Vision Co., Nanjing, China), and then imported into a blender to build the frame of the 3-dimensional PA. Then, all of the nerve endings were completely combined with the 3-dimensional PA model.

MEASUREMENTS OF SNCV. Of the 35 dogs, 10 dogs with mPAP ≤25 mm Hg and the remaining 25 animals with PAH were then used for an SNCV measurement and electron microscope assessment after PADN (Figure 1). To exclude the effect of DHMCT on SNCV, we measured SNCV in 6 normal animals without injection of DHMCT.

Following thoracotomy, the PA adventitia was carefully separated from the PA, with precautions undertaken to avoid damaging the nerves. The PA sympathetic nerves were isolated and connected to stimulator (2 mm proximal to the injured site) and sensor (2 mm distal to the injured site) probes with aeration. The distance between the sensor and stimulator probes varied from 10.0 to 17.2 mm. A digital storage oscilloscope (Tektronix 2211, Madell Technology Co., Ontario, California) was used to record the conduction times (3 to 5 V stimulation and 5 ms duration).

ULTRASTRUCTURAL CHANGES IN THE SN. The SNs were dissected (from the entry point, almost at the ostium of the main PA, to 2 mm distal to the orifice of the left branch) for electron microscopy. The nerves were immersed in fixative (2.5% glutaraldehyde) and incubated at 4°C for 12 h. Each specimen was then immersed in 2% osmium tetroxide for 2 h at 4°C and then dehydrated and embedded. Following polymerization, sections were cut and stained with uranyl acetate and lead citrate. The SN morphology was examined (JEM 1010, JEOL, Tokyo, Japan), and the axon diameter and the thickness of the myelin sheath in the SN were measured.

IMMUNOHISTOCHEMISTRY. Immunohistochemistry has been described previously. In brief, paraffin-embedded lung tissues were sectioned (5-μm thickness). Deparaffinization, rehydration, and antigen retrieval were performed on the slides. Endogenous peroxidases, avidin, nonspecific protein binding, and biotin were blocked. Then, the sections were treated with polyclonal goat antimouse RELMα (1:200, R&D Systems, Minneapolis, Minnesota) antibodies overnight at 4°C. Finally, the slides were treated with rabbit antigoat biotinylated secondary antibodies, followed by a horseradish peroxidase reagent (Vectastain Elite ABC Kit, Vector Laboratories, Burlingame, California) for 30 min each at room temperature.

ASSESSMENT OF PA REMODELING. PA remodeling was assessed in a blinded fashion. Lung sections were stained with hematoxylin and eosin. Double staining for the von Willebrand factor and α-smooth muscle actin was performed to evaluate the muscularization of the pulmonary vessels. Then, peripheral vessels

FIGURE 1 Study Flowchart

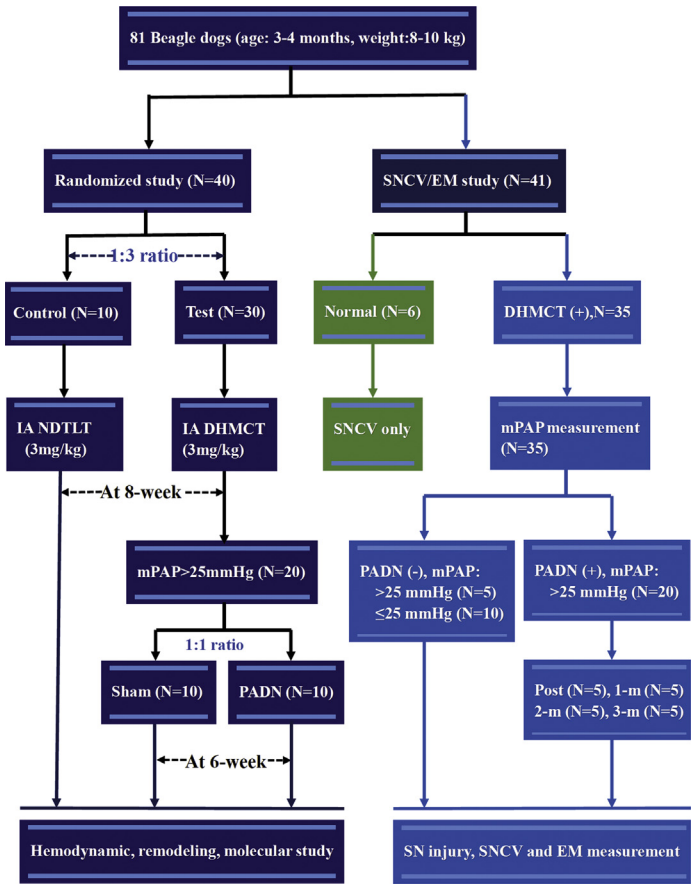

Eight weeks after the injection of dehydrogenized monocrotaline (DHMCT) (3 mg/kg), animals with mean pulmonary arterial pressure (mPAP) >25 mm Hg were randomized into the sham and pulmonary artery denervation (PADN) groups. Six weeks after the injection, repeated hemodynamic measurements and pulmonary artery (PA) remodeling were performed for all animals. Another 41 animals with or without injection of DHMCT were used to measure the sympathetic nerve conduction velocity (SNVC) and for electron microscopic (EM) assessments at different time points after PADN. IA = intra-atrial; NDTLT = N-dimethylacetamide; RHC = right heart catheterization; SN = sympathetic nerve.

FIGURE 2 **PADN Procedure, Lumen Lesion, and SN Injury**

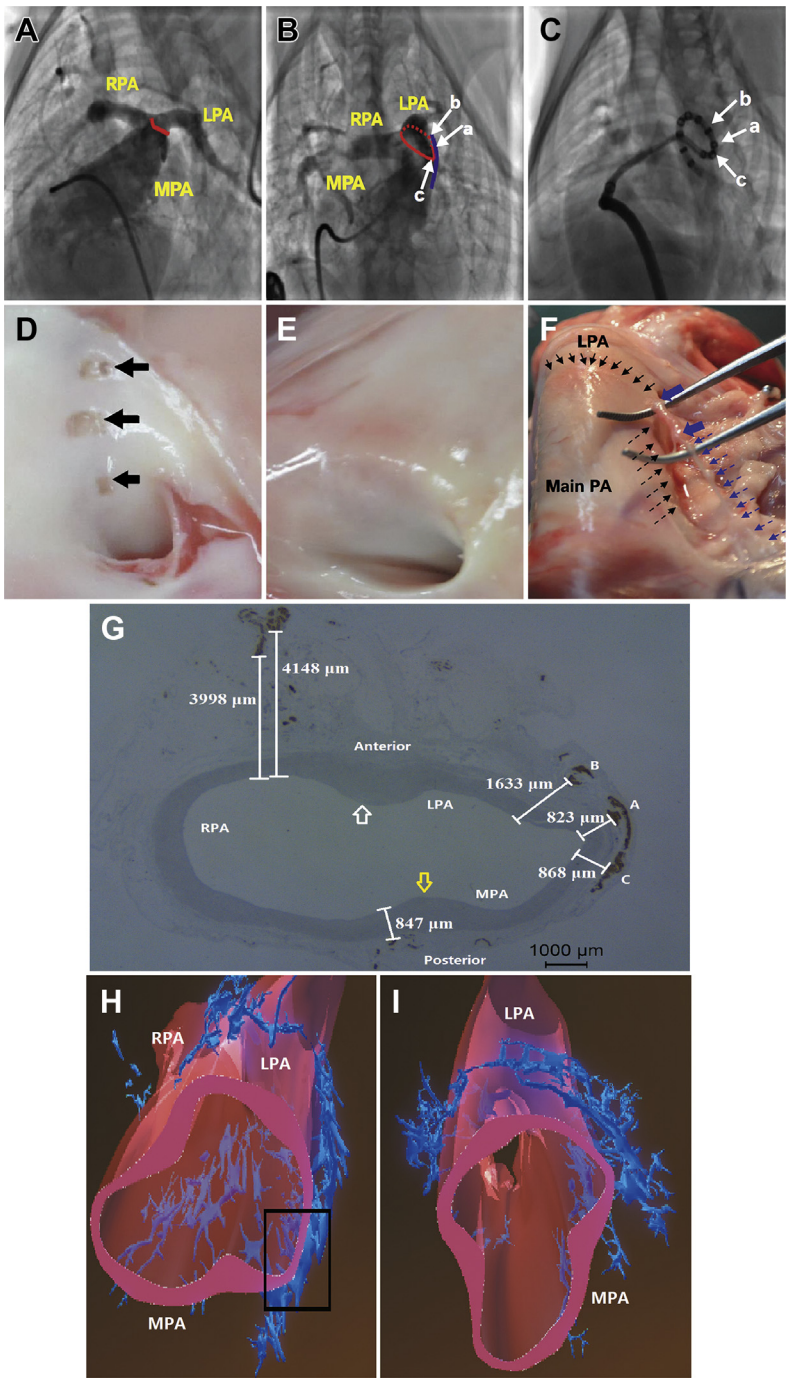

Pulmonary artery (PA) angiography of the left anterior cranial **(A)** and anterior-posterior cranial **(B)** view confirmed the position of the ostial left pulmonary artery (LPA) **(solid red circle)**, right pulmonary artery (RPA), lateral wall of the PA trunk **(green line in B)**, and posterior wall of the LPA **(dashed red line)**. The conjunction point of the main pulmonary artery (MPA) trunk lateral wall and ostial LPA was site b **(C)**. Sites a and c indicate the points located at the level of the distal main PA, 2 mm from site b. Immediately after PADN, an intimal injury was very clearly visualized **(black arrow in D)** and was replaced by scarring **(E)**. Sympathetic nerves localized in the groove **(dashed black arrows in F)** are parallel to the left lateral wall of the distal MPA up to the orifice of the LPA **(solid black arrows)**; when the nerves were removed from this groove, the injured segment induced by PADN **(solid blue arrows in F)** became swollen. **(G)** The shortest distance (823 μm) between the nerve endings and the PA lumen at the distal PA. The 3-dimensional reconstruction shows the distribution of the sympathetic nerve endings from the anterior-posterior view **(H)** and counter-clockwise rotation **(I)**. Abbreviations as in Figure 1.

from each dog were analyzed under an Olympus-BHS microscope (San Jose, California) attached to a QImaging Retiga 4000RV digital camera (Surrey, British Columbia, Canada). Muscularization was classified as non-, partial, or full. The percentage of medial wall thickness (%MWT) was calculated as: % MWT = ([external diameter − internal diameter]/ external diameter) × 100.

REAL-TIME QUANTITATIVE POLYMERASE CHAIN REACTION. Animal lung tissue was homogenized in RLT buffer, total ribonucleic acid was extracted using an RNeasy mini kit (Qiagen, Germantown, Maryland), and real-time quantitative polymerase chain reaction was performed according to the manufacturer's instructions.

STATISTICAL ANALYSIS. The continuous variables are expressed as the mean ± SD. A normality test for

TABLE 1 Sympathetic Nerve Conduction Velocity, Axon Diameter, and Myelin Thickness in Animals With and Without mPAP >25 mm Hg

	n	SNCV (m/s)	Axon Diameter (μm)	Myelin Thickness (μm)
Normal animals	6	14.15 ± 2.30	2.15 ± 0.28	0.37 ± 0.01
mPAP ≤25 mm Hg	10	40.33 ± 5.08*	5.27 ± 0.41†	1.13 ± 0.03*
mPAP >25 mm Hg	25			
Prior to PADN	5	48.07 ± 4.77‡	5.98 ± 0.20‡	1.62 ± 0.05‡
After PADN	20			
Post-PADN	5	37.99 ± 3.33§	4.75 ± 0.48§	0.87 ± 0.06§
1 month	5	26.34 ± 4.94‖	3.53 ± 0.29¶	0.62 ± 0.05¶
2 months	5	17.82 ± 4.85¶	3.51 ± 0.33¶	0.55 ± 0.06¶
3 months	5	13.05 ± 3.76	3.13 ± 0.19	0.39 ± 0.05

Values are mean ± SD. *p < 0.001, compared with all groups; †p < 0.01, compared with prior to PADN group and normal animals; ‡p < 0.001, compared with all subgroups in after PADN group; §p < 0.001, compared with 1, 2, and 3 months groups; ‖p < 0.01, compared with mPAP ≤25 mm Hg, 2 months, and 3 months groups; ¶p < 0.05, compared with the 3 months group.

mPAP = mean pulmonary arterial pressure; PADN = pulmonary artery denervation; SNCV = sympathetic nerve conduction velocity.

FIGURE 3 Ultrastructural Change, SNCV, Axon Diameter, and Myelin Thickness

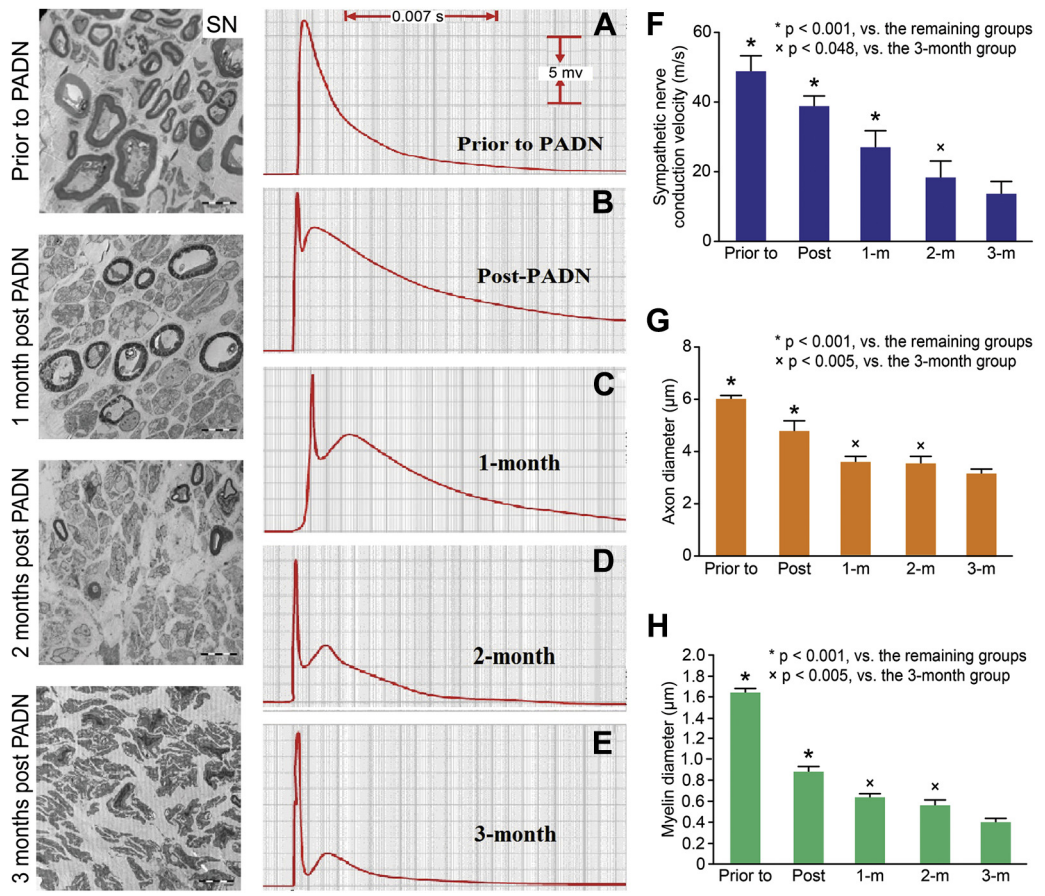

Before PADN, the myelin appeared smooth, and the mean SNCV was 48.1 m/s **(A to F)**, with a mean myelin thickness of 1.62 μm **(G)** and an axon diameter of 5.98 μm **(H)**. After the PADN procedure, the myelin thickness gradually decreased and was almost demyelinated by 3 months (SN). This result is consistent with the reduction of SNCV and axon loss. Abbreviations as in Figure 1.

FIGURE 4 Hemodynamic Changes

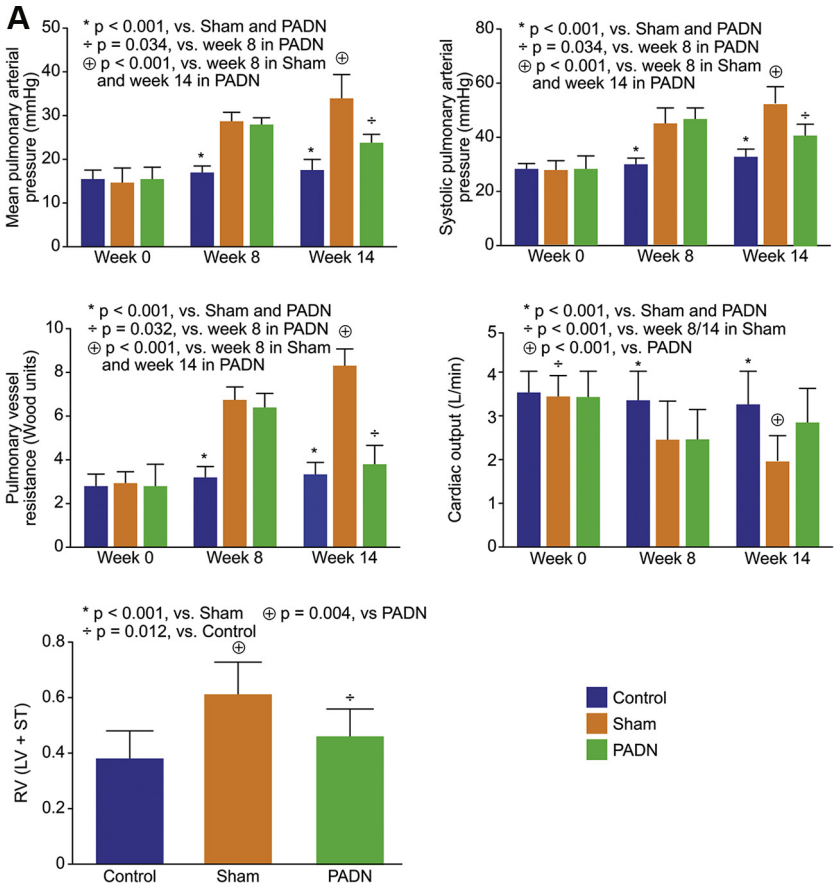

(A) Injection of dehydrogenized monocrotaline induced a significant increase in the mean and systolic pulmonary arterial pressure and the pulmonary vessel resistance at 8 weeks, which continuously increased over time in the sham group, but decreased significantly 6 weeks after the pulmonary artery denervation (PADN) procedure. PADN was associated with a significant reduction of right ventricular (RV) mass/(left ventricle [LV] + interventricular septum [ST]). Individual changes in the mean pulmonary arterial pressure (mPAP), pulmonary vessel resistance (PVR), and cardiac output (CO) are shown in **B**.

Continued on the next page

all of the continuous variables was performed using the Kolmogorov-Smirnov and Shapiro-Wilk tests. The differences in the continuous variables between the 2 treatments were analyzed using a paired *t* test or the Mann-Whitney *U* test when appropriate. Post-hoc analysis using Bonferroni's method was used to compare the 3 groups. The categorical variables were compared using the Fisher exact test. Statistical significance was defined as a 2-sided p value <0.05. All analyses were performed using the statistical program SPSS version 19.0 (SPSS Institute Inc., Chicago, Illinois).

RESULTS

PAH MODEL AND MORTALITY. Eight weeks after injection with DHMCT, the PAH model was successfully established in 20 dogs (67%) in the test group. A total of 4 deaths occurred after the second randomization, with 3 in the sham group and 1 in the PADN group. Finally, the sham group contained 7 dogs, and the PADN group contained 9 animals.

PADN PROCEDURE. PADN was performed at 3 sites (Figures 2A to 2C). The median procedural time was 7.5 min (interquartile range: 6 to 16 min). Immediately after PADN, the ablated sites were clearly observed on the intima of the PA (Figure 2D); these sites were sealed and replaced by a scar at 1 month (Figure 2E). No procedure-related complications occurred.

VISUAL ASSESSMENT OF SN INJURY. The noninjured SN had a smooth surface (Figure 2F, dashed blue

FIGURE 4 Continued

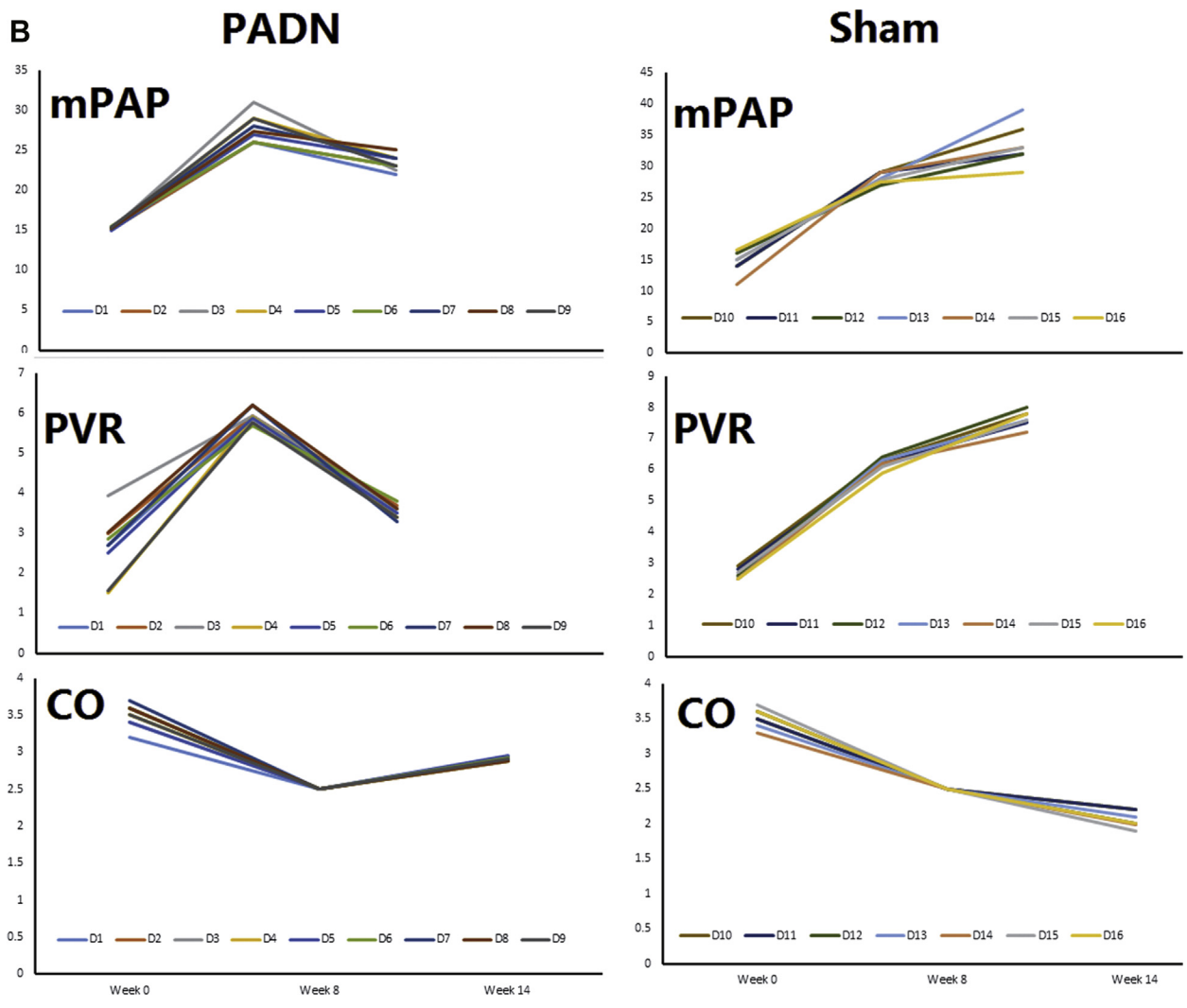

arrows). Immediately after PADN, the ablated segment became swollen (Figure 2F, solid blue arrows), which was in line with an intimal injury (Figure 2E).

DISTRIBUTION OF SYMPATHETIC NERVES. PA sympathetic nerve bundles were localized in the groove parallel to the left lateral side of the main PA trunk (Figure 2F) and were mostly bifurcated into the posterior wall of the main PA and LPA, with very few in the anterior wall of the right PA. The shortest distance from the nerves to the PA lumen was 823 μm, and the longest distance was 4,148 μm (Figures 2G to 2I).

SNCV MEASUREMENTS. SNCV was 14.15 ± 2.30 m/s in normal animals, 40.3 m/s in animals with an mPAP ≤25 mm Hg, and 48.1 m/s in animals with an mPAP >25 mm Hg, respectively (Table 1, Figure 3A). After the PADN procedure, the SNCV decreased very rapidly over time (Figures 3B to 3F).

ELECTRON MICROSCOPIC ASSESSMENT OF SN. Most nerve endings in animals with mPAP >25 mm Hg had smooth and relatively thick myelin (Figures 3, left panels [SN]), with a mean myelin thickness of 1.62 μm and a mean axon diameter of 5.98 μm (Figures 3G and 3H), significantly higher than those (5.27 and 1.13 μm, respectively) in animals with mPAP ≤25 mm Hg (Table 1). After the PADN procedure, the myelin sheath became noticeably thinner and the vacuoles degenerated over time (Table 1), with axon diameters significantly decreased to 3.53

TABLE 2 Changes in the Hemodynamics and PA Remodeling in the 3 Groups

	Control (n = 10)	PADN (n = 9)	Sham (n = 7)
Heart, beats/min			
Week 0	148 ± 25	147 ± 15	150 ± 17
Week 8	139 ± 23*	159 ± 21	159 ± 22
Week 14	134 ± 27†	160 ± 22	159 ± 24
RAP, mm Hg			
Week 0	1.7 ± 0.9	1.9 ± 1.3	1.7 ± 0.9
Week 8	2.0 ± 1.0‡	2.7 ± 2.5§	2.7 ± 1.2
Week 14	1.9 ± 0.9†	2.3 ± 0.8‖	3.2 ± 0.9
RVSP, mm Hg			
Week 0	32.0 ± 3.7	32.7 ± 7.1	32.4 ± 7.0
Week 8	33.4 ± 3.4†	49.0 ± 4.0§	49.1 ± 6.8
Week 14	36.0 ± 4.3†	44.9 ± 6.9‖	55.8 ± 5.7
sPAP, mm Hg			
Week 0	27.9 ± 2.2	27.6 ± 5.3	27.3 ± 3.8
Week 8	29.9 ± 2.3†	46.3 ± 4.3§	45.2 ± 5.5
Week 14	32.2 ± 3.0†	40.6 ± 4.6‖	52.1 ± 6.6
mPAP, mm Hg			
Week 0	15.3 ± 2.2	15.3 ± 3.0	14.4 ± 3.6
Week 8	16.9 ± 1.7†	27.7 ± 1.9§	28.6 ± 2.2
Week 14	17.3 ± 2.8†	23.5 ± 2.3‖	33.7 ± 5.8
Cardiac output, l/min			
Week 0	3.6 ± 0.5	3.5 ± 0.6	3.5 ± 0.5
Week 8	3.4 ± 0.7*	2.5 ± 0.7	2.5 ± 0.9
Week 14	3.3 ± 0.8†	2.9 ± 0.8‖	2.0 ± 0.6
PVR, Wood units			
Week 0	2.6 ± 0.5	2.6 ± 0.9	2.7 ± 0.5
Week 8	2.9 ± 0.5†	5.9 ± 0.6¶	6.2 ± 0.6
Week 14	3.1 ± 0.5†	3.5 ± 0.7#	7.7 ± 0.7
MWT at week 14, %	11.8 ± 1.2‖	22.3 ± 3.3‖	30.4 ± 4.1
Muscularization at week 14, mean ± SD of %			
None	59.1 ± 9.7†	29.8 ± 6.1‖	12.9 ± 4.9
Partial	29.4 ± 9.8	29.8 ± 9.7	30.3 ± 3.7
Fully	11.5 ± 2.6†	40.3 ± 9.3‖	57.1 ± 5.7

Values are mean ± SD. *p = 0.005 compared with the PADN and sham groups; †p < 0.001 compared with the PADN and sham groups; ‡p = 0.008 compared with the PADN and sham groups; §p < 0.05 compared with value measured at week 14; ‖p < 0.001 compared with the sham group; ¶p < 0.01 compared with value at week 14; #p = 0.005 compared with the sham group.

mPAP = mean pulmonary arterial pressure; MWT = medial wall thickness; PA = pulmonary artery; PVR = pulmonary vessel resistance; RAP = right atrial pressure; RVSP = right ventricular systolic pressure; sPAP = systolic pulmonary arterial pressure.

μm at 1 month. By 3 months post-PADN, the myelin sheath was almost invisible (Figure 3, left panels [SN], Figure 3G), and the nerve endings became demyelinated (Figure 3H).

HEMODYNAMIC CHANGE. The baseline hemodynamic variables were similar among the 3 groups (Figure 4A, Table 2) and were stably sustained in the control group, but increased continuously in the sham group during the 14-week follow-up period. PADN was associated with significant reductions of mPAP, systolic pulmonary arterial pressure, and right atrial pressure, and increased CO, leading to a significant reduction of pulmonary vessel resistance compared with the sham group. Finally, RV hypertrophy, by means of the ratio of the RV mass/(left ventricle + septal), in the PADN group was significantly lower than in the sham group (Figure 4A). The individual data of mPAP, pulmonary vessel resistance, and CO are shown in Figure 4B.

PA REMODELING. The %MWT in the PADN group was 22.3 ± 3.3%, significantly lower than that in the sham group (30.4 ± 4.1%, p < 0.001) (Table 2, Figure 5A). The rates of NM and full muscularization in the Sham group were 12.9 ± 4.9% and 57.1 ± 5.7%, respectively, significantly different from the PADN group 29.8 ± 6.1% and 40.3 ± 9.3%, respectively (all p < 0.001) (Figure 5B). There was no significant difference in partial muscularization between the sham and PADN (p = 0.057) groups.

REAL-TIME QUANTITATIVE POLYMERASE CHAIN REACTION. DHMCT-exposure was characterized by overexpression of platelet-derived growth factor-subunit B, fibroblast growth factor-2, endothelin-1, endothelial nitric oxide synthase, and monocyte chemoattractant protein-1 (Figure 6). These alterations were significantly less in the treatment group.

DISCUSSION

This study reports, for the first time, that: 1) the PADN procedure induces severe SN injury characterized by significant SN demyelination, axon loss, and slowing of SNCV over time; and 2) the PADN procedure results in significant improvements in hemodynamics and simultaneous PA remodeling in an experimental PAH model by inhibiting inflammation, abnormal proliferation, and vasoconstriction of pulmonary vascular beds.

The PA is surrounded by adventitia, which is loosely organized (8). The pulmonary trunk receives innervation starting with bundles of large nerve trunks that diminish in size, so that at the level of the arterioles, there is only a single fiber (14), as confirmed by initial studies identifying dense nerve endings at the proximal and bifurcated areas (15). We found nerves located in the conjunctional area between the left lateral wall of the main PA trunk and the ostial LPA. This anatomic structure suggested the possibility of achieving percutaneous ablation at these conjunctional sites via heat generated from the high-frequency alternating current (20). The intimal lesions post-PADN were replaced by scars 1 month after the procedure, without thrombus formation.

FIGURE 5 Pulmonary Artery Remodeling

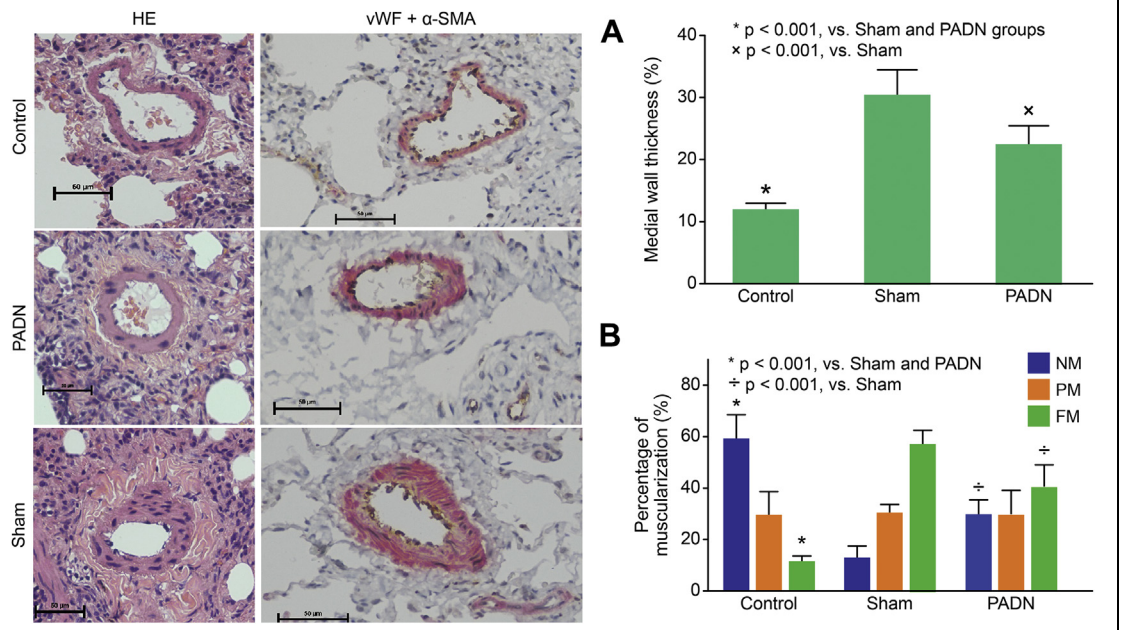

The smooth muscle layer appeared smooth and thin by hematoxylin and eosin (HE) and by von Willebrand Factor (vWF) and α-smooth muscle actin (SMA) staining. In the sham group, the percentage of medial wall thickness increased **(A)**, with a significant reduction in nonmuscularization (NM) and increase in full muscularization (FM) **(B)** compared with the pulmonary artery denervation (PADN) group. PM = partial muscularization.

Myelin protects the axons from injury and promotes the conduction of neuroelectrical stimuli (21). However, there has been no data clearly showing the changes in myelin and axon diameters of SN in the presence of PH or systematic hypertension. Our results demonstrate for the first time increased SNCV, myelin, and axon diameters in a DHMCT-induced PH model. From our results, SNCV in normal animals (no injection of DHMCT) was similar to previous reports (22,23), but we also found increased SNCV in animals without PAH (mPAP ≤25 mm Hg) after injection of DHMCT, which might indicate that DHMCT induced PAH via different mechanisms when compared with chronic hypoxia-induced PAH (24) and that 8-week follow-up was relatively shorter for these non-PAH animals. Given the truth that a monocrotaline model does not truly mimic severe PH as observed in humans (24–27), our results should be interpreted cautiously.

One of the key issues with the PADN procedure is whether permanent SN injury could be achieved by the ablation. Herein, visual assessment confirmed the severe nerve injury induced by PADN, as evidenced by severely swollen SN at the ablated segment. Furthermore, electron microscopy demonstrated that demyelination and axon loss of the SN started immediately after the PADN procedure, resulting in a prolonged conduction time and the loss of nerve potential amplitude. Those results clearly showed the efficacy of PADN in inducing persistent nerve injury in the surrounding tissues of the PA.

The proliferation of PA smooth muscle cells, leading to the increased muscularization of tiny arterioles and reduced vascular lumen, is the hallmark of PAH (1–3,15). The reverse of this pathological process is the primary endpoint of testing for potential therapies in animal models (25,26). Previous data revealed that SN overactivation was strongly correlated with the severity and prognosis of PAH (9–11) and that nebivolol, a β_1-antagonist and $\beta_{2,3}$-agonist, caused a significant improvement of endothelial function and PA remodeling in animals with monocrotaline-induced PAH (27). Overstimulation of adrenergic β_1-receptors in PAH leads to vessel constriction caused by impaired endothelial dysfunction, inflammation, and oxidative stress (9,10,27). The profound reduction in the muscularization of the small PA after PADN, as demonstrated by our study, is consistent with the improvement in hemodynamics and might be directly related to the SN injury induced by ablation. However, nerves in the adventitia of the PA and lung surrounding tissues consist of different

FIGURE 6 mRNA Expression Assessed by RT-qPCR

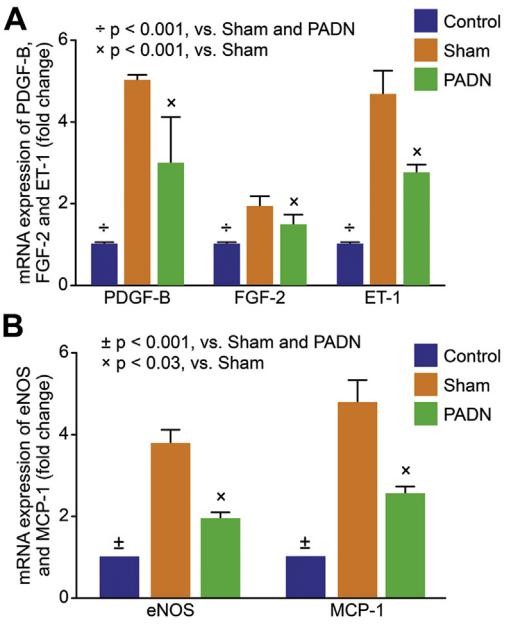

Dehydrogenized monocrotaline-induced pulmonary arterial hypertension (PAH) animal models displayed a significant up-regulation of growth factors endothelin-1 (ET-1) **(A)**, endothelial nitric oxide synthase (eNOS), and monocyte chemoattractant protein (MCP)-1 **(B)**. All of these changes were significantly improved by pulmonary artery denervation (PADN). FGF = fibroblast growth factor; mRNA = messenger ribonucleic acid; PDGF-B = platelet-derived growth factor-subunit B; RT-qPCR = real-time quantitative polymerase chain reaction.

nervous fibers (8,14,15), which release catecholamine, acetylcholine, histamine, neuropeptide-Y, and others. These neurotransmitters and cotransmitters are delivered to the pulmonary vasculature and induce vessel constriction and proliferation of smooth muscle cells (14,15). As a result, 1 positive effect of PADN is the inhibition or block of most (if not all) of the transmitters released from different nerves. However, a great deal of work remains to be done to identify the complex mechanisms for PADN.

Molecular studies (7,26,27) have shown that growth factors synthesized by many different cell types, coupled with an increase of endothelial nitric oxide synthase (causing endothelial dysfunction and apoptosis resistance) (28–30), endothelin-1 (31), and monocyte chemoattractant protein-1 (27), play an important role in the pulmonary vascular remodeling process responsible for the progression of PAH. Our finding that PADN attenuates PA remodeling by inhibiting abnormal cell growth is consistent with a previous study using nebivolol (26); however, the latter study did not find the reduction of fibroblast growth factor-2 after a high dose of nebivolol, indicating that PADN, by inducing an injury to all nerves (within reasonable distance of the vessel wall), led to the blockage or inhibition of most (if not all) transmitters released from the different nerves. Nevertheless, further work is required to elucidate the status of apoptosis resistance after the PADN procedure.

CLINICAL RELEVANCE. PAH is a severe disease. Sympathetic overactivation plays a critical role in the process of PAH. Our study demonstrated the improvements in hemodynamic, PA remodeling, and cardiac function after the PADN procedure. These benefits of PADN for PAH patients need to be testified by future clinical studies.

STUDY LIMITATIONS. First, the current study selected beagle dogs to establish a PAH model because the PADN catheter required a larger PA. In contrast to studies using small animal models, the success rate of establishing the PADN model in dogs was relatively reduced (~70%). However, in the present study, dogs with mPAP ≤25 mm Hg were excluded from the study for PA remodeling. Next, our study did not provide insights into the effect of PADN on different transmitters and the protein phosphorylation of signal molecules. However, our preliminary data unmasked the mechanisms of PA remodeling improvement by PADN. Third, the fraction of inspired oxygen was not collected in this study. Finally, the DHMCT-induced PAH model did not represent human PAH in terms of pathological changes (29). Further work will be required to test the efficacy of PADN in other PAH models.

CONCLUSIONS

Our results report that PADN induces SN injury and improves hemodynamics and PA remodeling, and provide the associated molecular mechanisms. Further studies are required to fine-tune the methodology of the ablation and to elucidate the long-term efficacy in different PAH models.

ACKNOWLEDGMENTS The authors deeply appreciate the assistance of Mr. Zhi-Guo Zheng (Polmono Company, Wuxi, China), who provided all of the PADN devices.

REPRINT REQUESTS AND CORRESPONDENCE: Dr. Shao-Liang Chen, Cardiology Department, Nanjing First Hospital, Nanjing Medical University, 68 Changle Road, Nanjing 210006, China. E-mail: chmengx@126.com.

PERSPECTIVES

WHAT IS KNOWN? SN overactivity plays a critical role in PAH. PADN was tested in experimental PAH and patients.

WHAT IS NEW? Our results reported the improvement and mechanisms of PA hemodynamic, remodeling, and cardiac function after PADN.

WHAT IS NEXT? Further studies are required to confirm our finding.

REFERENCES

1. Galiè N, Hoeper MM, Humbert M, et al., for the ESC Committee for Practice Guidelines. Guidelines for the diagnosis and treatment of pulmonary hypertension: the Task Force for the Diagnosis and Treatment of Pulmonary Hypertension of the European Society of Cardiology (ESC) and the European Respiratory Society (ERS). Eur Heart J 2009;30:2493–537.

2. Bogaard HJ, Abe K, Vonk Noordegraaf A, Voelkel NF. The right ventricle under pressure: cellular and molecular mechanisms of right-heart failure in pulmonary hypertension. Chest 2009; 135:794–804.

3. Voelkel NF, Quaife RA, Leinwand LA, et al., for the National Heart, Lung, and Blood Institute Working Group on Cellular and Molecular Mechanisms of Right Heart Failure. Right ventricular function and failure: report of a National Heart, Lung, and Blood Institute Working Group on Cellular and Molecular Mechanisms of Right Heart Failure. Circulation 2006;114: 1883–91.

4. Galiè N, Manes A, Negro L, Palazzini M, Bacchi-Reggiani ML, Branzi A. A meta-analysis of randomized controlled trials in pulmonary arterial hypertension. Eur Heart J 2009;30:394–403.

5. Humbert M, Sitbon O, Chaouat A, et al. Survival in patients with idiopathic, familial, and anorexigen-associated pulmonary arterial hypertension in the modern management era. Circulation 2010;122: 156–63.

6. Savarese G, Paolillo S, Costanzo P, et al. Do changes of 6-minute walk distance predict clinical events in patients with pulmonary arterial hypertension? A meta-analysis of 22 randomized trials. J Am Coll Cardiol 2012;60: 1192–201.

7. Gomberg-Maitland M, Bull TM, et al. New trial designs and potential therapies for pulmonary artery hypertension. J Am Coll Cardiol 2013;62: D82–91.

8. Verity MA, Bevan JA. Fine structural study of the terminal effecror plexus, neuromuscular and intermuscular relationships in the pulmonary artery. J Anat 1968;103:49–63.

9. Velez-Roa S, Ciarka A, Najem B, Vachiery JL, Naeije R, van de Borne P. Increased sympathetic nerve activity in pulmonary artery hypertension. Circulation 2004;110:1308–12.

10. Ciarka A, Doan V, Velez-Roa S, Naeije R, van de Borne P. Prognostic significance of sympathetic nervous system activation in pulmonary arterial hypertension. Am J Respir Crit Care Med 2010;181: 1269–75.

11. Wensel R, Jilek C, Dörr M, et al. Impaired cardiac autonomic control relates to disease severity in pulmonary hypertension. Eur Respir J 2009;34:895–901.

12. So PP, Davies RA, Chandy G, et al. Usefulness of beta-blocker therapy and outcomes in patients with pulmonary arterial hypertension. Am J Cardiol 2012;109:1504–9.

13. Provencher S, Herve P, Jais X, et al. Deleterious effects of beta-blockers on exercise capacity and hemodynamics in patients with portopulmonary hypertension. Gastroenterol 2006;130: 120–6.

14. Richardson JB. Nerve supply to the lungs. Am Rev Respir Dis 1979;119:785–802.

15. Townsley MI. Structure and composition of pulmonary arteries, capillaries, and veins. Compr Physiol 2012;2:675–709.

16. Juratsch CE, Jengo JA, Castagna J, Laks MM. Experimental pulmonary hypertension produced by surgical and chemical denervation of the pulmonary vasculature. Chest 1980;77: 525–30.

17. Chen SL, Zhang YJ, Zhou L, et al. Percutaneous pulmonary artery denervation completely abolishes experimental pulmonary arterial hypertension in vivo. EuroIntervention 2013;9:269–76.

18. Chen SL, Zhang FF, Xu J, et al. Pulmonary artery denervation to treat pulmonary arterial hypertension: the single-center, prospective, first-in-man PADN-1 study (first-in-man pulmonary artery denervation for treatment of pulmonary artery hypertension). J Am Coll Cardiol 2013;62:1092–100.

19. Galiè N, Manes A. New treatment strategies for pulmonary arterial hypertension: hopes or hypes? J Am Coll Cardiol 2013;62:1101–2.

20. Townsend CM, Beauchamp RD, Evers BM, Mattox KL. Sabiston Textbook of Surgery: the Biological Basis of Modern Surgical Practice. 19th edition. Philadelphia, PA: Elsevier Saunders, 2012:236.

21. Aramideh M, Ongerboer de Visser BW. Brainstem reflexes: electrodiagnostic techniques, physiology, normative data, and clinical applications. Muscle Nerve 2002;26:14–30.

22. Nishi K, Sakanashi M, Takenaka F. Activation of afferent cardiac sympathetic nerve fibers of the cat by pain producing substances and by noxious heat. Pflugers Arch 1977;372:53–61.

23. Nishi K, Sakanashi M, Takenaka F. Afferent fibres from pulmonary arterial baroreceptors in the left cardiac sympathetic nerve of the cat. J Physiol 1974;240:53–66.

24. Maarman G, Lecour S, Butrous G, Thienemann F, Sliwa K. A comprehensive review: the evolution of animal models in pulmonary hypertension research: are we there yet? Pulm Circ 2013;3:739–56.

25. Gomez-Arroyo JG, Farkas L, Alhussaini AA, et al. The monocrotaline model of pulmonary hypertension in perspective. Am J Physio Lung Cell Mol Physiol 2012;302:1363–9.

26. O'Callaghan DS, Savale L, Montani D, et al. Treatment of pulmonary arterial hypertension with targeted therapies. Nat Rev Cardiol 2011;8: 526–38.

27. Perros F, Ranchous B, Izikki M, et al. Nebivolol for improving endothelial dysfunction, pulmonary vascular remodeling, and right heart function in pulmonary hypertension. J Am Coll Cardiol 2015; 65:668–80.

28. Kraus DS, Van Etten RA. Tyrosine kinase as targets for cancer therapy. N Engl J Med 2005; 353:172–87.

29. Balasubramaniam V, Le Cras TD, Ivy DD, Grover TR, Kinsella JP, Abman SH. Role of platelet-derived growth factor in vascular remodeling during pulmonary hypertension in the ovine fetus. Am J Physiol Lung Cell Mol Physiol 2003;284:L826–33.

30. Izikki M, Guignabert C, Fadel E, et al. Endothelial-derived FGF2 contributes to the progression of pulmonary hypertension in humans and rodents. J Clin Invest 2009;119:512–23.

31. Sharma S, Sud N, Wiseman DA, et al. Altered carnitine homeostasis is associated with decreased mitochondrial function and altered nitric oxide signaling in lambs with pulmonary hypertension. Am J Physiol Lung Cell Mol Physiol 2008;294:L46–56.

KEY WORDS electron microscopy, pathological remodeling, pulmonary arterial hypertension, pulmonary artery denervation, sympathetic nerves